Nonlinearity 3 (1990) 361–386. Printed in the UK

Recycling of strange sets: II. Applications

Roberto Artuso†§, Erik Aurell‡ and Predrag Cvitanović†‖

† Niels Bohr Institute, Blegdamsvej 17, DK-2100 Copenhagen Ø, Denmark
‡ Institute of Theoretical Physics, Chalmers University of Technology and University of Göteborg, S-412 96 Göteborg, Sweden

Received 30 October 1989
Accepted by I Procaccia

Abstract. Cycle expansions are applied to a series of low-dimensional dynamically generated strange sets: the skew Ulam map, the period-doubling repeller, the Hénon-type strange sets and the irrational winding set for circle maps. These illustrate various aspects of the cycle expansion technique; convergence of the curvature expansions, approximations of generic strange sets by self-similar Cantor sets, effects of admixture of non-hyperbolicity, and infinite resummations required in presence of orbits of marginal stability. A new exact and highly convergent series for the Feigenbaum δ is obtained.

PACS numbers: 0320, 0545

1. Introduction

The goal of this paper is to demonstrate through a series of applications that description of low-dimensional chaotic systems in terms of unstable periodic orbits (cycles), advocated in the preceding paper [1] (hereafter referred to as I), is not only feasible, but that the cycles are indeed a powerful tool for analysis of deterministic chaos.

Our main tools are the cycle expansions (developed in the preceding paper) of the dynamical ζ functions [2]:

$$1/\zeta = \prod_p (1 - t_p) = 1 - \sum_f t_f - \sum_p c_p \tag{1}$$

which we apply to a series of examples with increasingly richer spectrum of scales. We test here the curvature expansions on much of the low-dimensional chaos; 1D repellers, 1D strange attractors, 1D period doublings, circle map mode lockings, 2D repellers and the Hénon strange attractors. The paper is organised as follows.

In section 2 we test the convergence of cycle expansions on the 'skew Ulam' map, which has complete binary symbolic dynamics and full measure but is non-hyperbolic and exhibits a first-order phase transition.

In section 3 we check explicitly the curvature estimates of paper I on an analytically tractable fractional linear repeller.

§ Present address: Dipartimento di Fisica dell'Università and INFN, Via Celoria 16, I-20133 Milano, Italy.
‖ Carlsberg Fellow.

0951-7715/90/020361+26$03.50

The knowledge of locations of the non-leading zeros and poles of ζ functions can lead to a dramatic improvement in the convergence of cycle expansions. We illustrate this in section 4 by applying these techniques to the period-doubling presentation function [3]. An unanticipated by-product is a new, highly convergent series for the Feigenbaum δ.

In section 5 we first apply the cycle expansions to the two-dimensional hyperbolic Lozi [4] map with non-trivial scaling and symbolic dynamics. We then test the cycle expansions on the non-hyperbolic Hénon mapping [5] which is believed to exemplify much of the generic structure of intertwining of order and chaos expected in general dynamical systems.

In section 6 we use the circle map mode-locking dynamics as a convenient testing ground for the applicability of cycle expansions to problems with coexisting regions of stability and chaos.

2. Skew Ulam mapping

In this section we apply the cycle expansion to a 'skew' Ulam map (figure 1) of the form

$$x' = \lambda x(1-x)(1-bx) \qquad 1/\lambda = x_c(1-x_c)(1-bx_c). \tag{2}$$

We shall refer here to any unimodal map for which the critical point x_c is mapped onto the unstable fixed point $x_0 = 0$ as a 'Ulam' map.

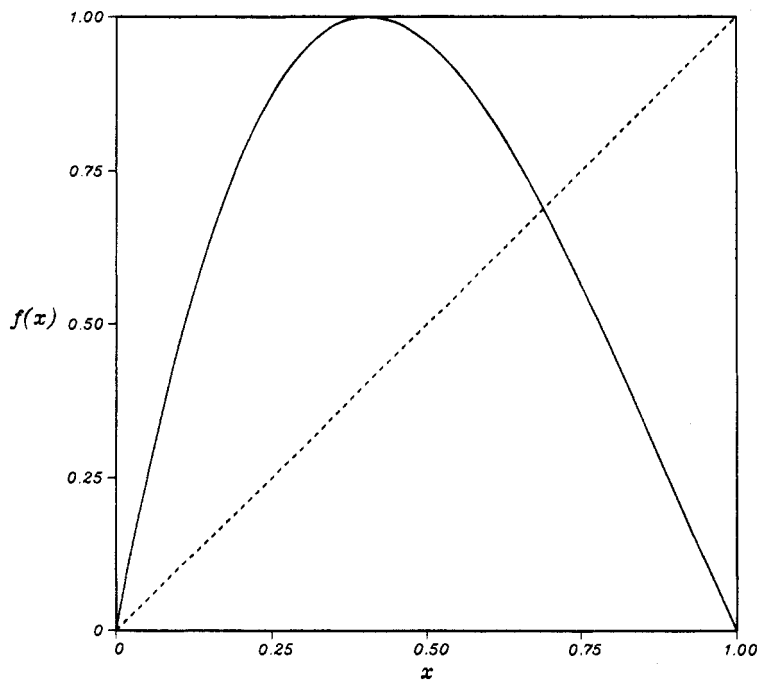

Figure 1. The skew Ulam map $f(x) = \lambda x(1-x)(1-bx)$, $1/\lambda = x_c(1-x_c)(1-bx_c)$, is a simple example of a strange attractor. Here $b = 0.6$.

In our numerical work we fix (arbitrarily) $b = 0.6$. Such a map is a convenient starting point for testing cycle expansions for several reasons:

(1) in the $b = 0$ limit it reduces to the parabola Ulam map (I.37), whose ζ function is available in explicit analytic form.

(2) the symbolic dynamics is a complete binary symbolic dynamics, and all cycles can be easily determined with a combination of inverse iterations and the Newton method; we have computed all cycle eigenvalues up to length 14;

(3) the nth iterate of the map generates a complete binary cover of the unit interval (see I, figure 2). The strange set has the full Lebesgue measure [6], so the cycle expansion estimates of the Hausdorff dimension can be tested against the exact value $D_H = 1$.

Due to the quadratic contraction around the critical point x_c, the mapping is *non-hyperbolic*. This is already clear from the parabola Ulam map (I.37), for which all cycles except $\overline{0}$ have eigenvalue $\Lambda_p = \pm 2^{n_p}$. Taking $t_p = \Lambda_p$, the nonlinearities (I.59) are

$$\frac{N_{ab}}{\Lambda_{ab}} \equiv \log \frac{t_a t_b}{t_{ab}} = \begin{cases} \ln 2 & \text{if } a \text{ or } b = 0 \\ 0 & \text{otherwise.} \end{cases} \tag{3}$$

The exact vanishing of the nonlinearity for the $a, b \neq 0$ case is an accident due to the fact that the Ulam parabola can be conjugated to the Ulam tent map; as we shall show here for the skew Ulam map (2), such nonlinearities in general fall off as Λ_{ab}^{-1}, as expected. More interesting is the fact that nonlinearities that involve t_0 counterterms do not fall off at all. This is the simplest example of the effects of non-hyperbolicity on the cycle expansions. The fixed point x_0 is singled out by the fact that the critical point x_c and all its pre-images (non-hyperbolic, as the critical point is supercontracting) map onto it. The number of fundamental cycles in the remaining Euler product $\prod'(1 - t_p)$ is infinite, as explained in section 5 of I. Such infinite sequences of fundamental cycles have to be resummed before the exponential convergence can be restored. In the Ulam example we already have the resummed $1/\zeta$ in closed form (I.38); in general such infinite summations have to be carried out numerically, but for the skew Ulam map the effect of non-hyperbolicity can still be accounted for rather easily. Consider the sequence of cycles of form $\overline{0\ldots01}$, consisting of k iterates by f_0 and one iterate by f_1, whose $x_{0\ldots01}$ cycle points accumulate to the x_0 fixed point. Here $f_0(x)$, $0 \leq x < x_c$, is the ascending branch of $f(x)$ in figure 1, and $f_1(x)$, $x_c < x \leq 1$, is the descending branch. The distance $\epsilon = x_{0\ldots01} - x_0$ can be estimated by noting that $f^{(k)}(x_{0\ldots01}) \approx \Lambda_0^k \epsilon \approx x_c$, so $\epsilon \approx 1/\Lambda_0^k$. The stability of the cycle $\Lambda_{0\ldots01} = f'(x_{0\ldots01}) \ldots f'(x_{010\ldots0}) f'(x_{10\ldots0})$ can be estimated by noting that $x_{01\ldots0}$, the point closest to x_c, is mapped quadratically into ϵ: $f(x_{01\ldots0}) = c(x_c - x_{01\ldots0})^2 + \ldots = \epsilon$, so $f'(x_{01\ldots0}) \approx \sqrt{\epsilon}$. Hence $\Lambda_{0\ldots01} \approx \Lambda_0^{k-2}\sqrt{\epsilon}\Lambda_1 \propto \Lambda_0^{k/2}$, and the stabilities of sequences of cycles of form $\overline{0\ldots01}$, and more generally $\Lambda_{0\ldots01\ldots}$, stabilities of cycles with a finite string of 0s and 1s followed by a long string of 0s, accumulate toward $\sqrt{\Lambda^k}$, and not toward Λ^k.

These estimates are borne out by the numerical results (figure 2). The effect of the non-hyperbolicity is to isolate the $\overline{0}$ fixed point, and the cycle expansion for the skew Ulam map is a slight generalisation of the exact $1/\zeta$ function (I.38) for the Ulam map:

$$1/\zeta(z) = \frac{(1 - t_0)}{(1 - t_0')} \prod_p{}' (1 - t_p) \tag{4}$$

where the cycle expansion of $\prod_p'(1 - t_p)$ is a complete binary expansion, but with t_0 replaced by t_0', where t_0' is the accumulation value $t_{00\ldots01} \propto t_0'^k$.

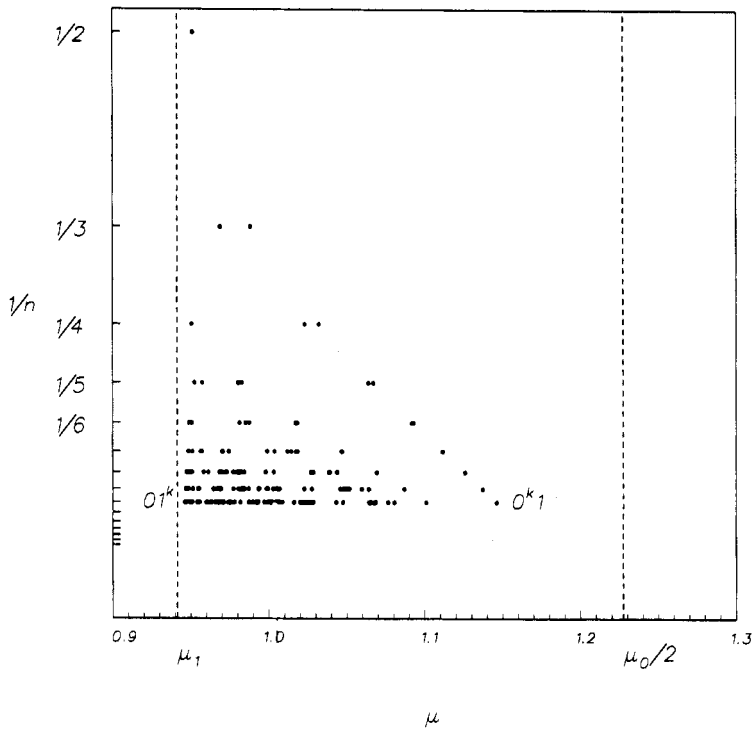

Figure 2. The distribution of the skew Ulam cycle Lyapunov exponents $\mu_p = \log|\Lambda_p|/n_p$. Due to the non-hyperbolic nature of the quadratic critical point x_c, μ_0 is isolated and all other cycle Lyapunov exponents are distributed between μ_1 and $\mu_0/2$.

As the first numerical check of the convergence of the cycle expansion (I.29) we compute the n-cycle estimates D_n of the Hausdorff dimension (I.84) by determining the leading zero of polynomial truncations of the cycle expansions of $0 = \prod'_p(1 - |\Lambda_p|^{-D_H})$ (figure 3). The geometric convergence of the D_n to the asymptotic value is evident, and relatively few cycles lead to extremely accurate estimates.

As the next check, we compute the thermodynamic functions $q(\tau)$ and $s(\mu)$ of I, section 9, with the equipartition measure $t_p = e^{\mu_p \tau} 2^{-n_p q}$. For the Ulam map (I.37) the thermodynamic behaviour can be immediately read off from the ζ function (I.38); $q(\tau)$ consists of two straight lines crossing at $\tau = 1$, where the zeros coincide, and a first-order phase transition takes place. The $q(\tau)$ function for the skew Ulam map is essentially the same; the slight spread of the cycle stabilities is more visible in the $s(\mu) = f(\alpha)/\alpha$ plot (figure 4). The computation of $f(\alpha)$ functions is straightforward, but the result is hardly as informative as the input information, the cycle stabilities (figure 2).

Parenthetically, while the above phase transition is a triviality from the ζ function point of view, the finite level sums $\sum p_i^q / l_i^\tau$ converge only logarithmically at the phase transition point [7] and the phase transition can be easily missed altogether in such averaging.

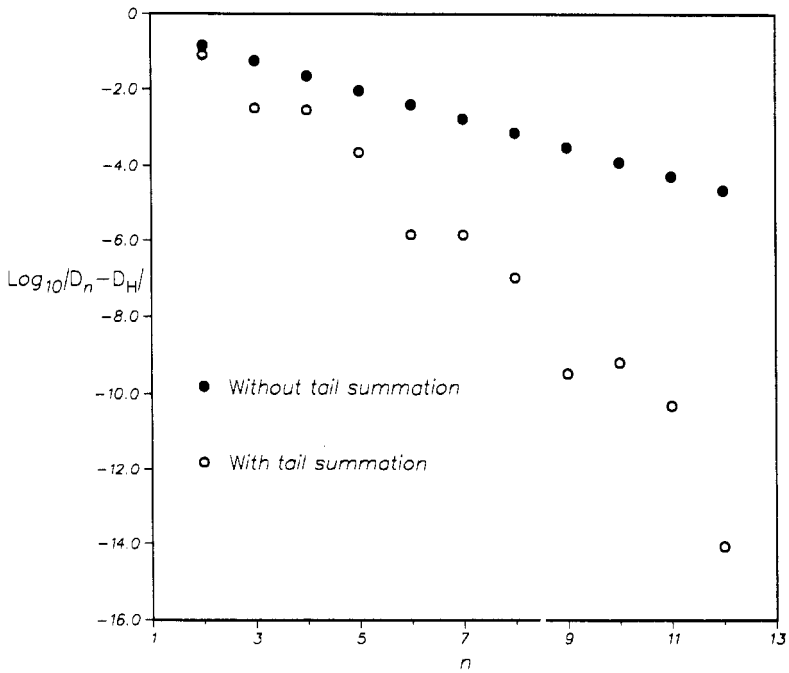

Figure 3. The convergence of the cycle expansion estimates of the Hausdorff dimension of the skew Ulam map strange attractor, evaluated by polynomial truncations. Plotted is the estimate error $\log_{10}|1 - D_n|$ as a function of the cycle length n. In spite of the non-hyperbolicity of the attractor, the convergence is exponential.

3. Curvature evaluation

In this section we check the curvature estimates of I, section 7 by explicit computation.

Consider a two-branch repeller of fractional linear form

$$\begin{aligned} f_0(x) &= \Lambda_0 x/(1+bx) \qquad -1/(b+\Lambda_0) \le x \le 0 \\ f_1(x) &= \Lambda_1(1+x) \qquad -1 \le x \le -1+\Lambda_1^{-1}. \end{aligned} \tag{5}$$

This is a repeller similar to the one depicted in I, figure 5. b parametrises the nonlinearity of the map: for $b = 0$ the repeller is a simple two-scale Cantor set (I.30). Fractional linear maps are well suited to analytical and numerical investigations, as their iterates remain fractional linear in form, and their periodic points are easily determined by solving quadratic equations (see section 6 for explicit examples). As an example we evaluate here the $t_{00\ldots1} - t_0 t_{0\ldots1}$ term in the curvature expansion (I.29). Let $a = 0\ldots1$. The $\overline{0a} = \overline{00\ldots1}$ cycle consists of k iterates by f_0

$$f_0^{(k)}(x) = \frac{\Lambda_0^k x}{1+b_k x} \qquad b_k = \frac{\Lambda_0^k - 1}{\Lambda_0 - 1} b$$

followed by a single f_1 iterate. The $x_{0a} = x_{00\ldots1}$ periodic point is a root of the quadratic equation

$$x = f_1 \circ f_0^{(k)}(x) = \Lambda_1 + \frac{\Lambda_0^k \Lambda_1 x}{1+b_k x}. \tag{6}$$

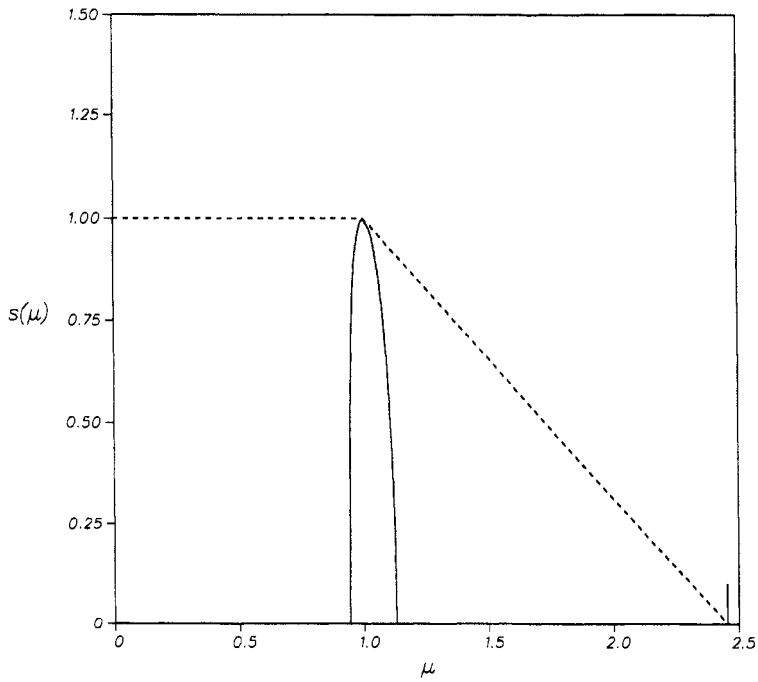

Figure 4. $s(\mu) = q(\tau) - \tau\mu(\tau)$ against $\mu(\tau) = dq/d\tau$ for the skew Ulam map with the equipartition measure $p_i = 2^{-n}$. In the thermodynamics extracted from finite $\sum p_i^q/l_i^\tau$ sums the right branch of $s(\mu) = f(\alpha)/\alpha$ is masked by the phase transition.

The stability of the $0a$ iterate is given by

$$f'_{0a}(x) = \frac{d}{dx}\left(f_1 \circ f_0^{(k)}(x)\right) = \frac{\Lambda_1 \Lambda_0^k}{(1 + b_k x)^2}.$$

Solving (6) to the leading orders in Λ_0^{-k} yields

$$x_{0a} = -\frac{\Lambda_1 y}{\Lambda_{0a}}\left[1 + \frac{1}{\Lambda_{0a}}\left(1 + \frac{b\Lambda_1 y}{\Lambda_0 - 1}\right)\right] + O(\Lambda_0^{-3k})$$

$$\Lambda_{0a} = f'_{0a}(x_{0a}) = \Lambda_0^k \Lambda_1 y^2 + O(1) \qquad y = 1 + \frac{b}{\Lambda_0 - 1}. \tag{7}$$

The two intervals on which the nonlinearity (I.59) is evaluated are $\Delta x_{0a} = x_0 - x_{0a} = -x_{0a}$ and $\Delta x_{a0} = x_a - x_{a0} = -(1/\Lambda_{0a}^2)\Lambda_0 \Lambda_1 (\Lambda_0 - 1)y$. The nonlinearity (I.60) depends on the choice of the weighting function $\varphi(x)$. If we take $\varphi(x) = f'(x)$, $t_0 = \Lambda_0$, the nonlinearity (I.60) is

$$N(x)\,dx = \frac{f''(x)}{f'(x)}\,dx. \tag{8}$$

Substituting

$$\Delta x_{a0} N_a(x_a) = -\frac{2b\Lambda_1 y}{\Lambda_{0a}} \qquad \Delta x_{0a} N_0(x_0) = -\frac{2b}{\Lambda_{0a}} \tag{9}$$

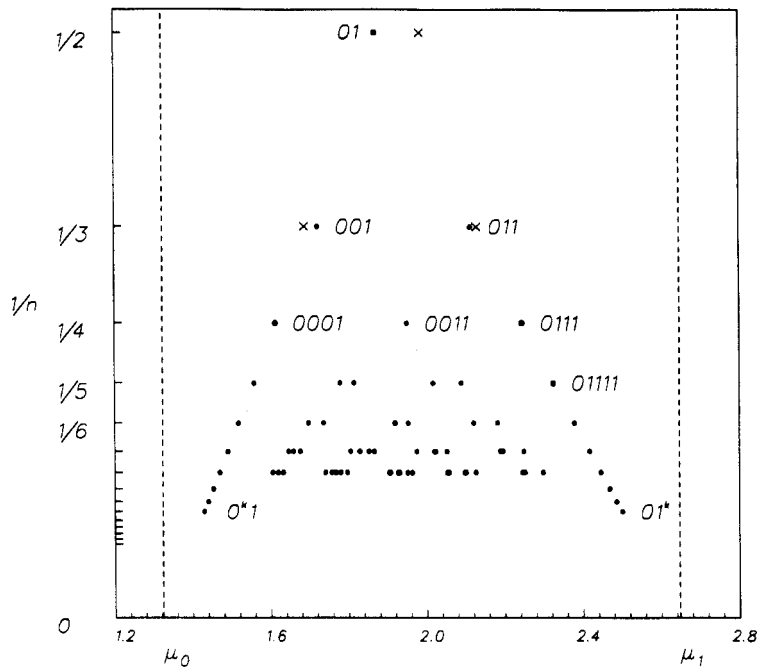

Figure 5. The distribution of the prime cycle eigenvalues for the period-doubling repeller (11), table 2: plotted are the cycle Lyapunov exponents $\mu_p = \log \Lambda_p / n_p \log 2$ against the inverse cycle length $1/n_p$. The regular structure arises from the approximate factorisation $\Lambda_p = \Lambda_0^{n_0} \Lambda_1^{n_1}$, where n_0 (n_1) is the number of 0s (1s) in the cycle p (compare with I, figure 3). A few shadowing estimates from shorter cycles, such as $\mu_{01} + \mu_0 \approx \mu_{001}$, are indicated by $\times$: the difference $\mu_{001} - \mu_{01} - \mu_0$ is a graphic illustration of curvatures (or the nonlinearity, in this case $\log(\Lambda_{01}\Lambda_0/\Lambda_{001})$).

into (I.59) we find that the curvature tends to a constant:

$$\Lambda_{0a} - \Lambda_0 \Lambda_a = 2b\left(\Lambda_1 - 1 + \frac{b\Lambda_1}{\Lambda_0 - 1}\right) + O(\Lambda_{0a}^{-1}). \tag{10}$$

The numerical verification of this estimate is given in table 1. Here $t_{0a}/\Lambda_{0a} = 1$, so the constant limit is in agreement with the estimate (I.62). This estimate can be trivially extended to weights such as $t_p = |\Lambda_p|^\tau$. The curvatures for the period-doubling repeller studied in the next section converge similarly, but in that case we lack explicit analytic expressions for the limits.

4. Period-doubling repeller

In this section we apply the cycle expansions to evaluation of the stability and the dimension of the period-doubling repeller. This strange set is interesting in its own right, but in the present context it is a convenient model for illustrating how the cycle expansions can be improved by using the information about the analytic structure of ζ functions.

Table 1. A comparison of the cycle eigenvalues Λ_p, the associated curvatures c_p and the estimate c_∞ from (10) for the fractional linear map (5), with parameters $b = -0.237\ 915\ 26$, $\Lambda_0 = -6.2645$ and $\Lambda_1 = 2.5029$.

p	Λ_p	c_p
100	−89.8514	−1.500 7569
1000	−561.2843	−1.593 9161
10000	−3 514.5827	−1.609 8959
100000	−22 015.6588	−1.612 4773
1000000	−137 916.5350	−1.612 8902
10000000	−863 983.1172	−1.612 9587
10.....000	∞	−1.612 9687

The period-doubling repeller is generated by the orbit of the critical point of a unimodal map at a 2^∞ parameter value. In the dynamical $x_{n+1} = f(x_n)$ variable, this set can be thought of as the $n \to \infty$ limit of 2^n attractive cycles in a period-doubling sequence. Alternatively, this set is the repeller of the period-doubling presentation function [3]

$$\begin{aligned} F_0^{-1}(x) &= \alpha g(x) \qquad && g\left(\alpha^{-1}\right) \le x \le 1 \\ F_1^{-1}(x) &= \alpha x \qquad && \alpha^{-1} \le x \le \alpha^{-2} \end{aligned} \tag{11}$$

where $g(x)$ is the universal period-doubling fix-point function which satisfies

$$g(x) = \alpha g \circ g(x/\alpha). \tag{12}$$

The stabilities

$$\Lambda_p = \frac{\partial F_p^{-1}(x_p)}{\partial x}$$

of the fixed points $x_0 = 1$, $x_1 = 0$ of (11) are $\Lambda_0 = \alpha^2$, $\Lambda_1 = \alpha$, where, for quadratic critical points, $\alpha = -2.502\ 907\ldots$. The stabilities of prime cycles up to length 6 are given in table 2 and figure 5. The presentation function (11) generates a nice hyperbolic repeller with complete binary symbolic dynamics, the variation in cycle stabilities is small (the slope of the F_0^{-1} branch is essentially α^2), and the cycle expansions are expected to converge swiftly.

4.1. The stability

In Sullivan's formulation of the period-doubling universality [8], the period-doubling repeller stability eigenvalue (as defined in I, section 8) is the Feigenbaum constant δ. This is easily checked by recasting the period-doubling fixed point linear stability equation [9], (obtained by substituting $g(x) \to g(x) + h_n(g(x))$ in (12)):

$$h_{n-1}(g(x)) = \alpha g'\left(g(x/\alpha)\right) h_n\left(g(x/\alpha)\right) + \alpha h_n\left(g(x)/\alpha\right) \tag{13}$$

into the presentation function form [3, 10]: substituting $g(x/\alpha) = g^{-1}\left(g(x)/\alpha\right) = F_0(g(x))$, $(1/\alpha)g(x) = F_1(g(x))$, we have

$$h_{n-1}(x_m) = \frac{\mathrm{d}F_0^{-1}(x_{0m})}{\mathrm{d}x} h_n(x_{0m}) + \frac{\mathrm{d}F_1^{-1}(x_{1m})}{\mathrm{d}x} h_n(x_{1m}) \qquad x_{\epsilon m} = F_\epsilon(x_m). \tag{14}$$

This is precisely the mother–daughter relation that led to the cycle expansion (I.71) for the stability of a strange set. In this context the cycle expansion

$$0 = 1 - (\alpha + \alpha^2)\delta^{-1} - (\Lambda_{01} - \alpha^3)\delta^{-2} - (\Lambda_{001} - \alpha^2\Lambda_{01} + \Lambda_{011} - \alpha\Lambda_{01})\delta^{-3} \ldots \tag{15}$$

is a new exact expansion for the Feigenbaum δ. Accurate estimates of δ are obtained by substituting values of short cycle eigenvalues α, Λ_{01}, Λ_{001}, Λ_{011}, ... (table 2). Using cycle expansions up to length 8, improved with the tail estimates, we obtain $\delta_{(8)} = 4.669\,201\,60\ldots$.

Table 2. The cycle eigenvalues and the associated curvatures (curvatures are defined in I, table 1) for the period-doubling presentation function. While the eigenvalues grow exponentially with the cycle length, the curvatures are roughly constant, in agreement with the estimate $c_p \approx t_p/\Lambda_p$.

p	Λ_p	c_p
1	−2.502 907 875 095 89	
0	6.264 547 831 217 04	
10	−13.369 876 879 005 5	−2.3097
100	−81.008 962 761 421 4	−2.7473
101	35.886 950 967 061 1	−2.4234
1000	−504.636 468 497 686	−2.8481
1001	222.899 012 688 299	−4.9597
1011	−87.409 121 049 762 8	−2.4126
10000	−3158.453 902 269 83	−2.8654
10001	1394.604 985 033 63	−5.3719
10010	1085.441 987 656 44	−2.3621
10011	−538.946 844 738 312	−3.8349
10101	−476.192 593 472 314	−3.6115
10111	221.198 178 025 952	−2.4212
100000	−19783.417 348 711 2	−2.8682
100001	8734.837 324 055 16	−5.4395
100010	6766.865 377 238 58	−5.1403
100011	−3367.974 049 464 22	−5.4395
100101	−2921.150 935 784 99	−11.3358
100110	−2938.097 905 469 20	
100111	1368.351 975 458 55	−4.2499
101110	1165.198 205 064 12	−5.5883
101111	−551.220 145 243 815	−2.4185

The numerical work supports the curvature estimates of I, section 7; table 2 illustrates the effect of replacing the cycle eigenvalues by the curvatures. While the cycle eigenvalues grow exponentially, in the present example the curvatures tend to constants.

The cycle expansions can be significantly improved by using information about the analytic structure of the ζ function. The curvatures of table 2 are individually small, but fluctuating. However, their sums are strikingly uniform, and the curvature ratios converge smoothly as $c_{n+1}/c_n \to 2$, in agreement with the conjecture of I, section 8, that $1/\zeta$ has a pole at $z = 1/2$. As illustrated in figures 6 and 7, the convergence of the $(1-2z)/\zeta$ expansion is considerably better than that of the $1/\zeta$ expansions, with the estimated radius of convergence now extended to $\delta \approx -4.57$. $(1-2z)/\zeta$ expansion indicates the next zero at $\delta_1 = 1$. We interpret this as the $\delta_1 = 1$ marginal eigenvalue [9] of (13), corresponding to a constant rescaling $g(x) \to (1.+h)g(x/(1+h))$. Dividing

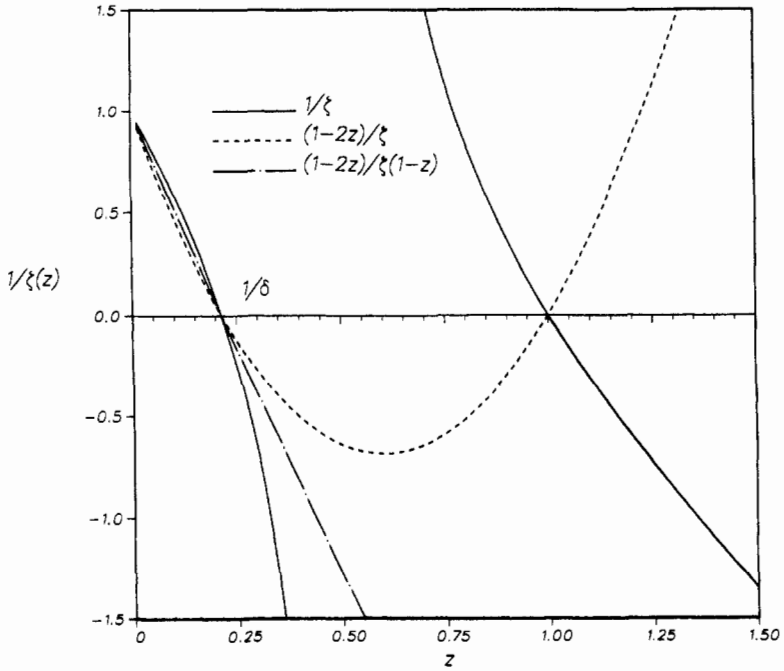

Figure 6. Incorporating the non-leading zeros and poles of ζ functions into the cycle expansion for the Feigenbaum δ improves the convergence of the leading pole $z = 1/\delta$ estimates. Full curve: the tail extrapolated $n = 8$ cycle expansion of the $1/\zeta$ function (15) for the stability of the period-doubling repeller. Broken curve: the cycle expansion of $(1-2z)/\zeta$, with the $z = 1/2$ pole removed. Chain curve: the cycle expansion of $1-2z/(1-z)\zeta$, with the non-leading zero at $z = 1$ removed as well.

explicitly out that root and expanding $(1-2z)/(1-z)\zeta$ as a power series in z we obtain a highly convergent expansion for the Feigenbaum δ:

$$0 = 1-(\alpha+\alpha^2+1)\delta^{-1}-(\Lambda_{01}-\alpha^3-\alpha^2-\alpha+1)\delta^{-2}+\dots . \tag{16}$$

Keeping only the terms up to δ^2 already yields three significant digits of δ: $\delta_{(2)} = 4.6647\dots$, as a root of a quadratic equation. Including the cycles up to length 8 and improving the convergence by tail estimates yields

$$\delta_{(8)} = 4.669\,201\,609\,102\,991\dots . \tag{17}$$

The convergence of the above cycle expansions is illustrated in figure 7; clearly, these are highly convergent expansions for determining the Feigenbaum δ.

4.2. The Hausdorff dimension

D_H, the Hausdorff dimension of the period-doubling repeller, is determined by (I.84):

$$0 = \prod_p \left(1-|\Lambda_p|^{-D_H}\right) = 1-\left(\frac{1}{|\alpha|^{D_H}}+\frac{1}{|\alpha^2|^{D_H}}\right)-\left(\frac{1}{|\Lambda_{01}|^{D_H}}-\frac{1}{|\alpha^3|^{D_H}}\right)-\dots$$

where Λ_p are the prime cycle eigenvalues listed in table 2. The cycle expansions converge very well—as we have already discussed at length this convergence, we here

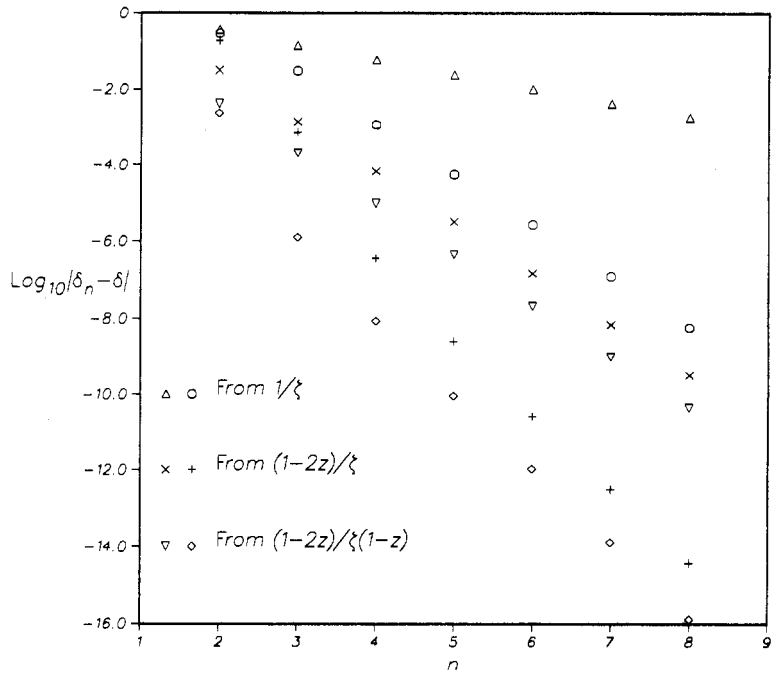

Figure 7. The convergence of the cycle expansions for the Feigenbaum δ, evaluated by polynomial truncations ($\triangle$, $\times$, ∇) and by tail extrapolations ($\bigcirc$, $+$, $\diamond$) from the cycle expansions of figure 6. Plotted is the estimate $\log_{10}|\delta_n - \delta|$ error as a function of the cycle length n, where $\delta = 4.669\ 201\ 609\ 102\ 991\ldots$ is our best estimate of the Feigenbaum δ. Note that the analytically improved cycle expansion (16) yields about *eight times* as many significant digits as the simple polynomial truncation of $1/\zeta$.

simply state the result. Including cycles up to length 8 and improving the convergence by tail estimates we get

$$D_{\mathrm{H}}^{(8)} = 0.538\ 045\ 1435\ldots$$

in agreement with the most accurate estimates available in the literature [11–14].

To summarise: cycle expansions applied to the period-doubling repeller converge extremely well, significantly faster than any other numerical evaluation of D_{H} and δ that we are familiar with. In addition they yield a new exact expansion for the Feigenbaum δ.

5. Hénon-type strange sets

The Hénon map [5]

$$\begin{aligned} x_{n+1} &= a - x_n^2 + y_n \\ y_{n+1} &= bx_n \end{aligned} \tag{18}$$

is the prototype of the stretching and folding dynamics that leads to deterministic chaos. It is a generic dynamical system, with arbitrarily complicated symbolic dynamics and

a mixture of hyperbolic and non-hyperbolic behaviours; the usefulness of the cycle expansions stands or falls on the extent to which they are applicable to such systems. We test them here in three steps: (1) on a purely hyperbolic Lozi map, with approximate symbol dynamics of a finite subshift type; (2) on a Hénon repeller with exact symbol dynamics of a finite subshift type; (3) on the canonical non-hyperbolic Hénon 'strange attractor', with no known finite grammar.

5.1. Lozi map

The piecewise linear Lozi map [4] is defined by

$$\begin{aligned} x_{n+1} &= y_n + (a-1) - a|x_n| \\ y_{n+1} &= bx_n. \end{aligned} \tag{19}$$

For this map the existence of a hyperbolic strange attractor has been rigorously established [15]. A binary symbolic dynamics is given by the y axis: we associate the symbol $\epsilon_n = 1$ with $x_n > 0$, and $\epsilon_n = 0$ with $x_n < 0$. A detailed analysis of the symbolic dynamics is contained in [16] to which we address the reader for further details: the main result that we rely on here is that it is possible to find parameter values for which we can approximate the strange set by symbol dynamics of a finite subshift type. In particular, for parameter values $a = 1.694\ 6978$ and $b = 0.064\ 262\ 36$ (which correspond to the simultaneous inverse bifurcation of the $\overline{100}$, $\overline{101}$ and $\overline{10011}$, $\overline{10010}$ cycles) the rules amount to forbidding the blocks $\_00100\_$, $\_01100\_$, $\_1000\_$ and $\_10011\_$. We have worked out this symbolic dynamics in I, section 5, example 6; the fundamental cycles are $\overline{1}$, $\overline{10}$, $\overline{10100}$ and $\overline{1011100}$, so we expect that the topological noisiness is absent with inclusion of the fundamental cycles, and for $n \geq 7$ we expect exponentially convergent curvature corrections.

This is confirmed by the Hausdorff dimension calculations, summarised in figure 8. As the attractor is hyperbolic, the measure is continuous along the unstable direction and the Hausdorff dimension is determined by a one-dimensional computation of the partial dimension (I.81) along the stable direction, $D_H = 1 + D_S$, with D_S given by

$$0 = \prod_p (1 - |\Lambda_p^s|^{D_S}). \tag{20}$$

Here Λ_p^s is the contracting (stable) eigenvalue of the cycle p. The hyperbolicity of the Lozi attractor guarantees good convergence of finite estimates for thermodynamical functions in their whole range: we have checked this numerically for $q = q(\tau)$ defined by

$$0 = \prod_p \left(1 - e^{-n_p q(\tau)} |\Lambda_p^s|^{-\tau}\right).$$

As illustrated by figure 9, the thermodynamic functions such as $s(\mu) = q(\tau) - \tau\mu(\tau)$, $\mu(\tau) = dq/d\tau$ (see (I.83)) are smooth and exponentially convergent over their entire range.

The Lozi map (19) with $b = 0.064\ 2636$ is almost one dimensional, so the excellent convergence of the above D_H calculation might be taken for granted. In fact, this convergence is by no means automatic, and *depends crucially* on the correct implementation of the symbolic dynamics (the topology) of the pruned strange set. This is

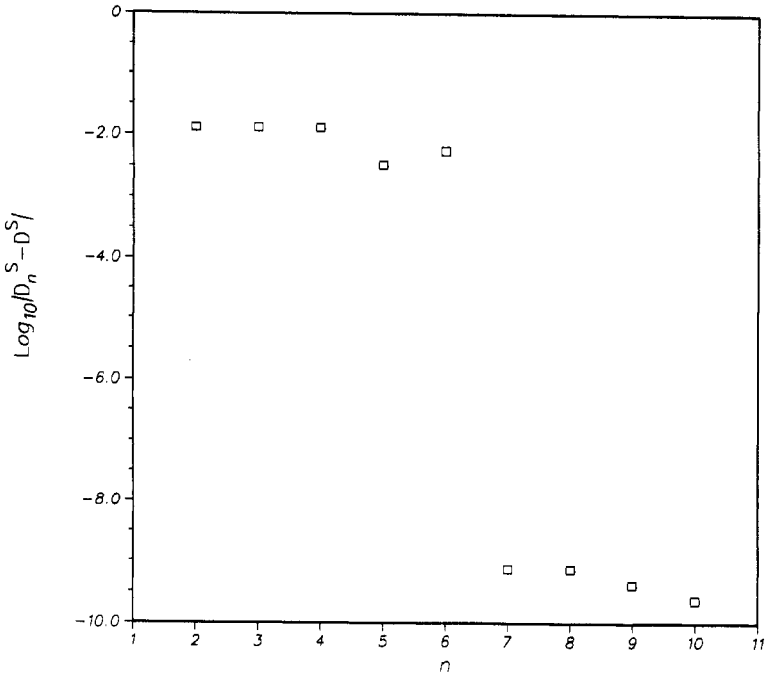

Figure 8. The convergence of polynomial truncations of the cycle expansion for the Hausdorff dimension of the Lozi map (19) strange attractor for parameter values a = 1.694 6978, b = 0.064 262 36. According to the grammar of I, section 5, example 6, the longest fundamental cycle is of length 7. With its inclusion, the curvature corrections take over, and the accuracy of the transverse dimension (20) estimate improves by 7 significant digits (D_S = 0.159 954 0649...).

the essential ingredient in applying the cycle expansions; as we shall see in the Hénon example discusssed below, the difference between a piecewise linear map, such as the Lozi map, and a continuous map, such as the Hénon map, is of secondary importance.

The problem is that the Lozi map is not structurally stable; any change of parameters, no matter how minute, can destroy or generate an infinity of cycles, and our symbol dynamics of a finite subshift type is only approximate. Violations are expected for long cycles; in this case none were found [17] up to cycle length 17. The implementation of the approximate symbol dynamics also requires some care. In particular, the pruning rules used here forbid the $\overline{100}$ and $\overline{10011}$ cycles, but require the companion $\overline{101}$ and $\overline{10001}$ cycles. For the Lozi map the pairs $\overline{100}$, $\overline{101}$ and $\overline{10011}$, $\overline{10001}$ are generated simultaneously precisely at the parameter values we work with. Furthermore, for the Lozi map the period-doubling cascades [17] such as the $\overline{100101}$, $\overline{100101100100}$, ..., period doublings of $\overline{100}$, are forbidden by the pruning rules, but are generated together with the $\overline{100}$, $\overline{101}$ bifurcation. The good convergence of the calculation (20) depends on implementing the finite subshift type symbolic dynamics, in this case by

(i) excluding the isolated $\bar{0}$ cycle from the cycle expansion

(ii) manually excluding the grammar violations $\overline{100}$, $\overline{10011}$, $\overline{100101}$, ... from the cycle expansion.

This is an example of implementing our strategy of approximating a generic (structurally unstable) strange set by a self-similar Cantor set.

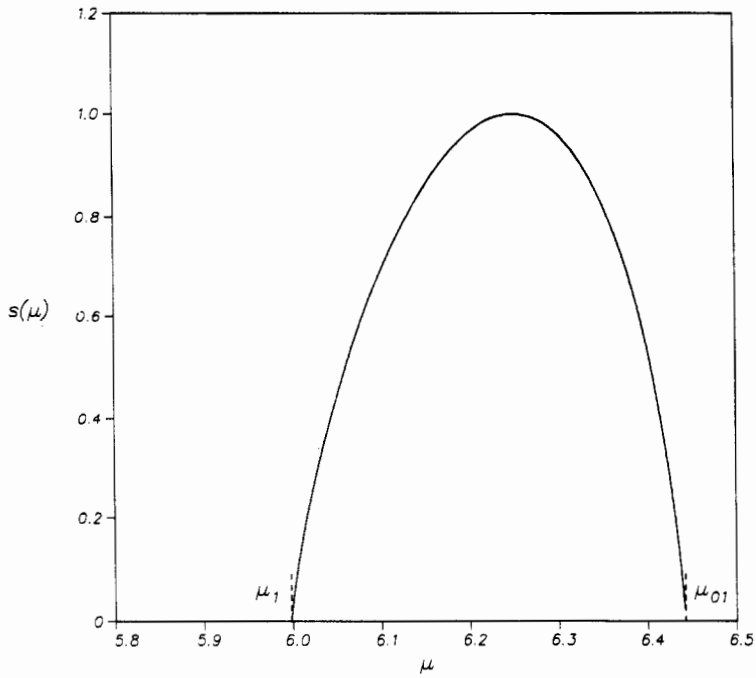

Figure 9. The $s(\mu) = f(\alpha)/\alpha$, $\mu = 1/\alpha$ plot for the Lozi map (19) strange attractor, $a = 1.694\ 6978$, $b = 0.064\ 262\ 36$.

5.2. *A Hénon repeller with a finite grammar*

As the next test of the applicability of the cycle expansions we consider the Hénon map (18) at parameter values $a = 1.812\ 5797$, $b = 0.022\ 8643$, introduced in [16]. At these parameter values the Hénon map has the same topology as the example just discussed above but, perhaps suprisingly, the Hénon map is easier to deal with than the Lozi map.

The difference is that here, unlike for the Lozi map, the strange set is a structurally stable repeller, and the grammar of I, section 5, example 6, is believed to be exact [18]. The reason is that at these parameter values both $\overline{100}$, $\overline{101}$ and the $\overline{10011}$, $\overline{10010}$ pairs exist, but only $\overline{101}$ and $\overline{10010}$ are unstable; the $\overline{100}$, $\overline{10011}$ are attractive cycles, enveloped by their immediate basins of attraction. These basins are conjectured to be sufficiently wide to cover all neighbouring primary folds, so that all remaining cycles are hyperbolic. The numerical work supports this; for example, with inclusion of the fundamental cycles the partial dimension (20) converges very well, see figure 10.

5.3. *The Hénon strange attractor*

The Hénon map (18), for Hénon's original choice of parameters $a = 1.4$, $b = 0.3$, is an example of a 'generic' dynamical system. It behaves numerically as a strange attractor, though the existence of a strange attractor at these parameter values is still a conjecture. A binary symbolic dynamics can be constructed using the primary turnbacks, or homoclinic tangencies [19]. No finite grammar is known to reproduce exactly the allowed symbol sequences and finite approximate grammars of increasing complexity that we advocate here have not yet been constructed. That means that at present the topology of the Hénon attractor is not under control. This is already

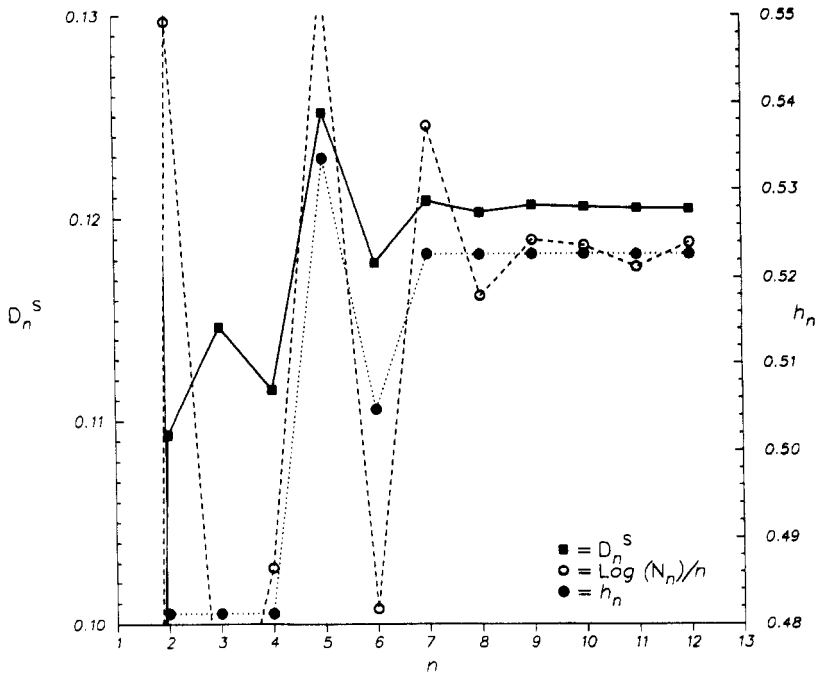

Figure 10. Cycle expansion estimates of the topological entropy (●) and the partial dimension (■) of the Hénon map (18) repeller for parameter values $a = 1.812\ 5797$, $b = 0.022\ 8643$. The topological entropy computed from the topological ζ function (I.47) becomes exact with the inclusion of all fundamental cycles (here with $n \geq 7$), while the $(\log N_n)/n$ estimate (○) continues oscillating irregularly for all n. The estimates of the partial dimension (I.86), (20) for the Hénon repeller follow the $n < 7$ oscillations of the topological entropy; for $n \geq 7$ the exponential convergence of the curvature corrections sets in ($D_S \approx 0.1205$).

reflected in the mediocre convergence of the topological entropy estimates (figure 11); the cycle expansion convergence is now not significantly better than the crude direct estimate $h_n = \log(N_n)/n$.

The Hénon $a = 1.4$, $b = 0.3$ strange attractor exemplifies the ways in which a cycle expansion applied blindly to a generic dynamical system fails to converge significantly better than other methods. This does not mean that the cycle expansions do not work; it simply means that a more careful analsis of the symbolic dynamics, beyond the scope of the present paper, is required.

The thermodynamic averages suffer from the same 'topological' noisiness as h_n, but in addition they are also affected by the non-hyperbolicity of the map; there are occasional longer and longer orbits which come closer and closer to turnbacks, and have anomalously low unstable eigenvalues and anomalously high measure. This is clearly illustrated by the figure 12 plot of $\mu = dq/\tau$ against τ for the partial dimension cycle expansion (I.81); from the cycle length 12 truncation to the cycle length 13 truncation of the cycle expansion, $\mu(\tau)$ goes through a violent jump for positive τ. This is caused by the nearly stable 13-cycle $\overline{1001110100110} = \overline{3112312}$ (for $a = 1.399\ 452\ 14$, $b = 0.3$ this cycle becomes a sink). In a generic non-hyperbolic system such anomalously nearly stable or stable cycles cannot be controlled, as infinitesimally small parameter changes can move arbitrarily long cycles onto contracting folds. However, for averages

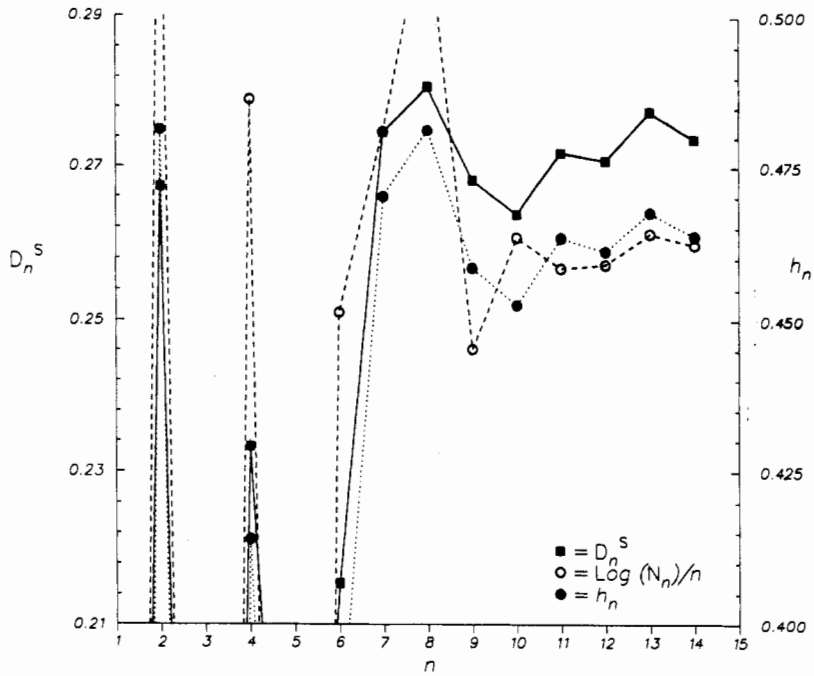

Figure 11. Cycle expansion estimates of the topological entropy (●) and the partial dimension (■) of the Hénon strange attractor, $a = 1.4$, $b = 0.3$. As the symbolic dynamics is not of a finite subshift type, the cycle expansion for the topological entropy does not converge significantly better than the direct $(\log N_n)/n$ estimate (○). Note that the oscillations in the estimates of the partial dimension (I.86), (20) track closely the oscillations in estimates of the topological entropy; non-hyperbolicity effects play a secondary role in controlling the convergence. Our estimate $D_H = 1.274 \pm 0.003$ is in agreement with previous estimates [36].

evaluated in the 'hyperbolic phase' [16, 20] (the parameter τ values for which the thermodynamic averages are dominated by the positive entropy of maximally unstable orbits) such nearly stable cycles are exponentially suppressed and cause only small perturbations. The maximally unstable orbits are under control, as they are smoothly bounded from above by regions of maximal expansion in the flow. For example, the 13-cycle estimate of the Hausdorff dimension D_H for the Hénon attractor is only a few per cent away from the best asymptotic estimate, in spite of the presence of the anomalous cycle.

We conclude that the cycle expansions for thermodynamic averages are expected to converge even for non-hyperbolic systems, provided that the average is evaluated in the hyperbolic phase. However, the presence of marginal orbits has important effects on the convergence of cycle expansions—we shall undertake a detailed investigation of such convergence in the next section.

6. Inclusion of marginal cycles

In this section we apply cycle expansions to a strange set with a mixture of hyperbolic and marginal orbits. The model that we shall use (the shift map, or the distribution of rationals on the unit interval) might at first glance appear trivial, but we find it very

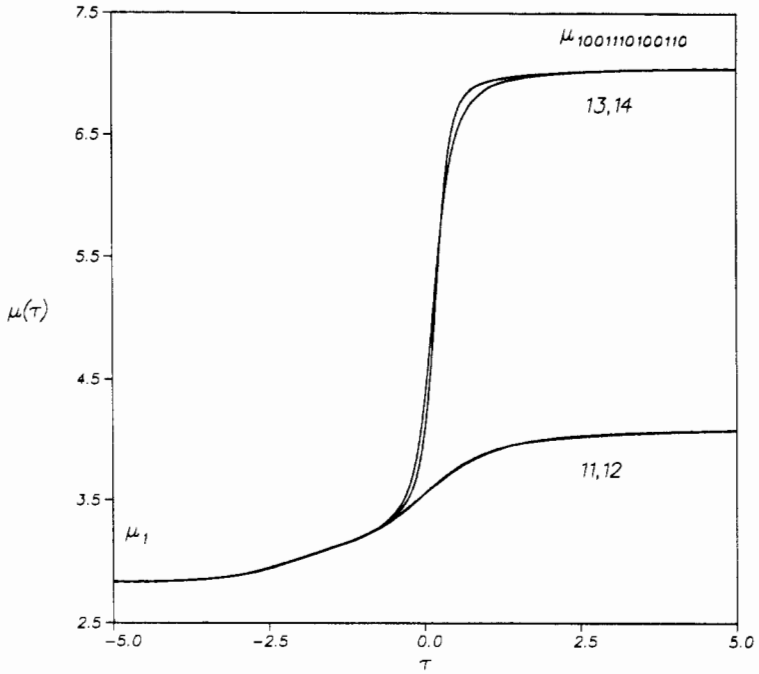

Figure 12. The effect of non-hyperbolicity (in this case, presence of a 13-cycle of anomalously low instability) of the Hénon attractor on thermodynamic averaging; $\mu(\tau) = dq/d\tau$ is dominated by the anomalous cycle for large positive τ, but barely affected by it for τ values in the 'hyperbolic phase'.

instructive: it illustrates how the cycle expansions developed here apply to strange sets with mixtures of hyperbolic and marginal stabilities. In such systems there are orbits that stay 'glued' arbitrarily close to stable regions for arbitrarily long times. This is a generic phenomenon in physically interesting dynamical systems, such as the Hamiltonian systems with coexisting elliptic islands of stability and hyperbolic homoclinic webs, and development of good computational techniques is here of utmost practical importance. The derivation of the dynamical ζ functions requires hyperbolicity, so only the cycles with expanding eigenvalues can be included into the cycle expansions. In our approach the presence of marginally stable cycles will be accounted for indirectly, in terms of infinite sums of cycles; for a different approach see [21].

In order to arrive at the example of such sums that we shall investigate here, we first have to introduce the 'mode-locking dynamics'. This unfortunatelly necessitates some notational detail, and cycle expansions and curvature corrections will resurface only at the end of this section.

The physical motivation behind study of circle maps is following; a typical island of stability in a Hamiltonian 2D map is an infinite sequence of concentric tori and chaotic rings. In the crudest approximation, the radius can be treated as an external parameter Ω, and the angular motion can be modelled by a map periodic in the angular variable, such as

$$x_{n+1} = x_n + \Omega - \frac{k}{2\pi}\sin(2\pi x_n) \bmod 1. \tag{21}$$

By losing all of the 'island-within-island' structure of real systems, such approximations skirt the problems of determining the symbolic dynamics for a realistic Hamiltonian

system, but they do retain some of the essential non-hyperbolicity of such systems in form of sequences of cycles accumulating toward the borders of stability.

In a Hamiltonian system we would be interested in sequences of KAM tori; in the circle map model their role is played by the *irrational winding set*, the set of parameter values for which the winding number $W = \lim_{n\to\infty} x_n/n$ takes irrational values. This set is of some experimental and theoretical interest in its own right. We shall study it here in the 'number-theoretic' limit $k \to 0$, with (21) reduced to the shift map

$$x_{n+1} = x_n + \Omega \qquad \text{mod } 1. \tag{22}$$

This map has a cycle of length Q for every rational $\Omega = P/Q$. If a nonlinear term is added to (22), the parameter region in which the winding number W maintains the rational value opens into a mode-locked interval [22] $\Delta_{P/Q}$. Deletion of a set of such mode-locked intervals Δ_{P_i/Q_i} leaves behind a set of complement intervals l_{P_i/Q_i} which provide a finite cover for the irrational winding set. For the shift map (22), the covering intervals are simply the differences of the consecutive rationals in the set of deleted $\{P_i/Q_i\}$;

$$l_{P_i/Q_i} = \frac{P_i}{Q_i} - \frac{P_{i-1}}{Q_{i-1}}. \tag{23}$$

A hierarchical presentation of the irrational winding set depends on the choice of organisation [23] of rationals on the unit interval. We describe here briefly two superficially rather distinct organisations; the Farey tree and the continued fraction partitioning of the unit interval. Actually, as we shall see, they are the same organisation, differing only in the choice of measure.

6.1. *Farey tree partitioning*

The Farey tree partitioning is a systematic bisection of rationals: successive levels are obtained by deleting from each subinterval the rational with the smallest denominator. It was introduced in [24–27] and its thermodynamics is discussed in detail in [3, 23], so here we simply state the rule that generates the tree; each rational (conveniently written in the continued fraction representation as $P/Q = [a_1 a_2 \ldots a_k]$) has 2 'daughters'

$$\begin{array}{ccc} & [\ldots, a] & \\ [\ldots, a-1, 2] & & [\ldots, a+1]. \end{array}$$

The nth level of the tree consists of all continued fractions satisfying $\sum a_i = n+2$; the nth level irrational winding cover consists of the 2^{n-1} intervals l_i obtained by deleting the corresponding mode-lockings up to the nth level. These intervals can be generated by iterating the Farey presentation function [3]:

$$\begin{aligned} f_0(x) &= x/(1-x) \qquad 0 \le x < 1/2 \\ f_1(x) &= (1-x)/x \qquad 1/2 < x \le 1 \end{aligned} \tag{24}$$

in the same way in which the unimodal map of I, figure 2 generates the covers of a two-branch repeller, and with the same binary symbolic dynamics. However, there is one crucial difference between the hyperbolic repeller of I, figure 2, and the Farey

presentation function; here the fix point $x_0 = 0$ has marginal stability $\Lambda_0 = 1$, and has to be excluded from the cycle expansions because it violates the hyperbolicity assumption used in the derivation of the ζ functions in I, section 2. Pruning $\overline{0}$ (setting $t_0 = 0$) unbalances all curvature combinations of form $t_{00\ldots1} - t_0 t_{0\ldots1}$, and turns $t_{00\ldots1}$ into fundamental cycles (cycles not shadowed by shorter cycles). The cycle expansion (I.29) becomes

$$\frac{1}{\zeta} = 1 - (t_1 + t_{01} + t_{001} + \ldots) - (t_{011} - t_{01}t_1) - (t_{0011} - t_{001}t_1)\ldots. \tag{25}$$

As there is an infinity of fundamental cycles, the binary Farey notation no longer seems particularly natural; a better choice is the continued fraction labelling. The transcription from the binary Farey labels to the continued fraction labels follows from the mother–daughter relation above; each block $1\ldots0$ ('1' followed by $a-1$ zeros) corresponds to entry $[\ldots,a,\ldots]$ in the continued fraction label. Functionally this corresponds to replacing the binary Farey presentation function f_0 in (24) by an infinity of branches

$$f_a(x) = f_1 \cdot f_0^{(a-1)}(x) = \frac{1}{x} - a \qquad \frac{1}{a-1} < x \leq \frac{1}{a} \tag{26}$$

and replacing the pruned binary expansion (25) by

$$1/\zeta = 1 - \hat{t}_1 - (\hat{t}_{12} - t_1\hat{t}_2) - (\hat{t}_{112} - t_1\hat{t}_{12}) - (\hat{t}_{23} - t_2\hat{t}_3) - (\hat{t}_{122} - t_{12}\hat{t}_2) - (\hat{t}_{1112} - t_1\hat{t}_{112}) - \ldots \tag{27}$$

where $\hat{t}_p$ stands for t_p together with its infinite tail sequence of cycles of form (see I, table 3)

$$\hat{t}_1 = \sum_{a=1}^{\infty} t_a \qquad \hat{t}_{12} = \sum_{a=2}^{\infty} t_{1a} \qquad \hat{t}_{a_1\ldots a_{k-1}a_k} = \sum_{a=a_k}^{\infty} t_{a_1\ldots a_{k-1}a}\,. \tag{28}$$

The thermodynamic sum (I.6) is in this context the sum over all rationals, labelled by binary Farey labels; transcribed to the continued fraction labelling it becomes

$$\Omega(z,\tau) = \sum_{k=1}^{\infty} \sum_{a_1,a_2,\ldots a_k}^{\infty} z^n l_{a_1a_2\ldots a_k}^{-\tau} \qquad n = \sum_{j=1}^{k} a_j. \tag{29}$$

The corresponding prime cycle weight in the cycle expansion (27) is

$$t_{a_1a_2\ldots a_k} = z^n |\Lambda_{a_1a_2\ldots a_k}|^{\tau} \qquad n = \sum_{j=1}^{k} a_j. \tag{30}$$

The associated thermodynamic functions and the slow convergence at the phase transition point for this thermodynamics are studied in detail in [23, 28]; we refer the reader to the above references for details of the Farey level thermodynamics and concentrate here on the Gauss partitioning.

6.2. Gauss map partitioning

An alternative to the Farey tree organisation of rationals is the continued fraction partitioning of the unit interval, obtained by deleting successively mode-locking intervals (points in our case) corresponding to continued fractions of increasing length. The first level is obtained by deleting $\Delta_{[1]}, \Delta_{[2]}, \ldots, \Delta_{[n]}, \ldots$ mode-lockings; the second by deleting $\Delta_{[1,2]}, \Delta_{[1,3]}, \Delta_{[2,2]}, \Delta_{[2,3]}, \ldots, \Delta_{[n,m]}, \ldots$ and so on (see figure 13). As in I, section 2, we form a partition sum over all levels

$$\Omega(z,\tau) = \sum_{n=1}^{\infty} z^n \sum_{a_1 a_2 \ldots a_n = 1}^{\infty} l_{a_1 a_2 \ldots a_n}^{-\tau} \tag{31}$$

where

$$l_{a_1 a_2 \ldots a_n} = |[a_1, a_2, \ldots, a_n] - [a_1, a_2, \ldots, a_n + 1]| = \frac{1}{Q_{[a_1,\ldots,a_n]} Q_{[a_1,\ldots,a_n+1]}}. \tag{32}$$

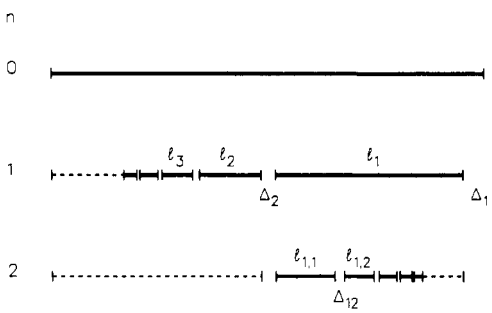

Figure 13. Continued fraction partitioning of the irrational winding set. At level $n = 1$ all mode locking intervals $\Delta_{[a]}$ with winding numbers 1/1, 1/2, 1/3, ..., 1/a, ... are deleted, and the cover consists of the complement intervals l_a. At level n=2 the mode locking intervals $\Delta_{[a,2]}, \Delta_{[a,3]}, \ldots$ are deleted from each cover l_a, and so on.

In contrast to the Farey tree case (30), in this *continued fraction thermodynamics* the infinity of intervals obtained by deleting continued fractions of length n are given the same weight $z^n = e^{-nq}$. The cycle expansion is (27), with the prime cycle weight

$$t_p = z^n |\Lambda_{a_1 a_2 \ldots a_n}|^{\tau}. \tag{33}$$

The intervals $l_{a_1 a_2 \ldots a_n}$ partition the parameter axis Ω, not the dynamical coordinate of the underlying circle map; still there exists a map that acts on the parameter space and generates the partition into intervals $l_{a_1 a_2 \ldots a_n}$. This map is known as the Gauss map [29] (see figure 14)

$$f(x) = \begin{cases} \dfrac{1}{x} - \left[\dfrac{1}{x}\right] & x \neq 0 \\ 0 & x = 0\,. \end{cases} \tag{34}$$

Here [...] denotes the integer part, and we note that this is actually the map (26) already introduced for the Farey tree. The Gauss map acts as a left shift on the continued fraction representation of numbers on the unit interval:

$$x = [a_1, a_2, a_3, \ldots] \rightarrow f(x) = [a_2, a_3, \ldots] \tag{35}$$

so it maps 'daughter' intervals $l_{a_1 a_2 \ldots a_n}$ into the 'mother' interval $l_{a_2 \ldots a_n}$ (see I, section 3).

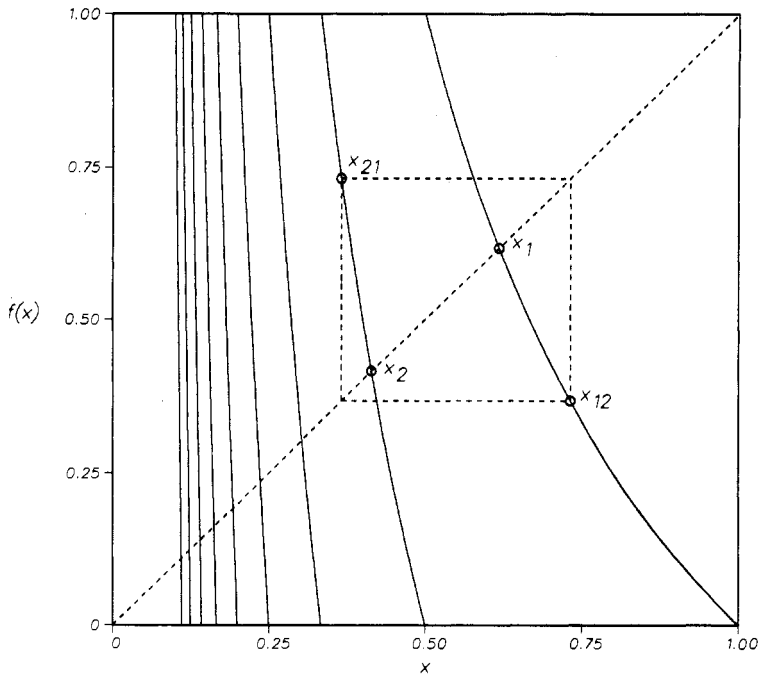

Figure 14. The Gauss map (34), with the fixed points x_1, x_2 and the $\overline{12}$-cycle indicated.

6.3. ζ *function from the Gauss measure*

For this simple toy model the transfer matrix (I.13) can be evaluated explicitly, using elementary properties of continued fractions. Let $P_n/Q_n = [a_1, a_2, \ldots a_n]$ be the leading edge of the $l_{a_1 a_2 \ldots a_n}$. Then

$$T_{dm} = \frac{l_{a_1 a_2 \ldots a_n a_{n+1}}}{l_{a_1 a_2 \ldots a_n}} = \frac{1 + P_n/Q_n}{(a_{n+1} + P_n/Q_n)(a_{n+1} + 1 + P_n/Q_n)} \tag{36}$$

and

$$\Omega(z,\tau) = \sum_{n=1}^{\infty} z^n \sum_{a_1 \ldots a_n}^{\infty} \prod_{k=1}^{n} \left(\frac{(a_{k+1} + P_k/Q_k)(a_{k+1} + 1 + P_k/Q_k)}{1 + P_k/Q_k} \right)^{\tau}. \tag{37}$$

We can take advantage of the ergodicity of the Gauss map and approximate the distribution of P_k/Q_k by an integral over the Gauss measure [29]. This yields a geometric series

$$\Omega(z,\tau) = \sum_{n=1}^{\infty} z^n \left(\frac{1}{\log 2} \sum_{m=1}^{\infty} \int_0^1 \frac{\mathrm{d}y}{1+y} \left(\frac{(m+1+y)(m+y)}{1+y} \right)^{\tau} \right)^n. \tag{38}$$

The corresponding ζ function [30] is

$$\frac{1}{\zeta(z,\tau)} = 1 - \frac{z}{\log 2} \sum_{m=1}^{\infty} \int_0^1 \frac{\mathrm{d}y}{1+y} \left(\frac{(m+1+y)(m+y)}{1+y} \right)^{\tau}. \tag{39}$$

For $\tau = -1$, $\zeta(z,-1)$ has a simple pole at $z = e^{-q} = 1$: i.e. the Hausdorff dimension (I.84) of the set of irrational numbers in the unit interval is 1, as it should be.

The above estimate of the ζ function was made possible by availability of the Gauss measure in explicit analytic form. However, as such measures are in general not available, we now return to the cycle expansion technique, in order to test its convergence in this analytically tractable model.

6.4. Cycles of the Gauss map

Given a symbol sequence $a_1, a_2, \ldots, a_n$, the corresponding cycle of the Gauss map can be computed by iterating the inverse Gauss map

$$f_a^{-1}(x) = \frac{1}{a+x} \qquad 0 \le x < 1 \qquad a \in Z^+ \tag{40}$$

where f_a^{-1} is the inverse of the $a = [1/x]$ branch of f in (34). The stability and the nonlinearity (I, section 7) of f^{-1} are

$$f_a^{-1}(x)' = -\frac{1}{(a+x)^2} \qquad \frac{f_a^{-1}(x)''}{f_a^{-1}(x)'} = -\frac{2}{a+x} \tag{41}$$

The cycle points satisfy

$$x_{a_1 a_2 \ldots a_n} = \frac{1}{a_1 + x_{a_2 \ldots a_n a_1}} \qquad \ldots \qquad x_{a_n a_1 a_2 \ldots} = \frac{1}{a_n + x_{a_1 a_2 \ldots a_n}} \tag{42}$$

the periodic points are determined by solving quadratic equations

$$x_{a_1 a_2 \ldots a_n} = x = \cfrac{1}{a_1 + \cfrac{1}{a_2 + \cdots \cfrac{1}{a_n + x}}} \tag{43}$$

and the Gauss map $\overline{a_1 a_2 \ldots a_n}$ cycle eigenvalue follows from (41) and (42) by the chain rule

$$\Lambda_{a_1 a_2 \ldots a_n} = (-1)^n (x_{a_1 a_2 \ldots a_n} x_{a_2 \ldots a_n a_1} \cdots x_{a_n a_1 a_2 \ldots a_{n-1}})^{-2}. \tag{44}$$

For example, the x_a fixed points (quadratic irrationals with $x_a = [a, a, a \ldots]$ infinitely repeating continued fraction expansion) are given by

$$x_a = \frac{-a + \sqrt{a^2+4}}{2} \qquad \Lambda_a = -\left(\frac{a + \sqrt{a^2+4}}{2}\right)^2 \tag{45}$$

and the $x_{ab} = [a, b, a, b, a, b, \ldots]$ 2-cycles are given by

$$x_{ab} = \frac{-ab + \sqrt{(ab)^2 + 4ab}}{2b} \tag{46}$$

$$\Lambda_{ab} = (x_{ab} x_{ba})^{-2} = \left(\frac{ab + 2 + \sqrt{ab(ab+4)}}{2}\right)^2.$$

This completes our discussion of the mode-locking dynamics; now we have all the ingradients necessary for evaluation of cycle expansions.

6.5. Cycle expansions

In the fixed-points approximation the cycle expansion (27) is given by

$$\zeta^{(1)}(z,\tau) = 1 - z\sum_{a=1}^{\infty} |\Lambda_a|^{\tau}\,. \tag{47}$$

The large a behaviour is the same as for the Riemann ζ function $\zeta(-2\tau) = \sum_{a=1}^{\infty} a^{2\tau}$. Indeed, (47) can be expanded as a finite sum plus a series of truncated Riemann ζ functions:

$$\zeta^{(1)}(z,\tau) = 1 - z\left[\sum_{a=1}^{N} |\Lambda_a|^{\tau} + \zeta_N(-2\tau) + 2\tau\zeta_N(2-2\tau) + (4\tau-3)\tau\zeta_N(4-2\tau) + O\left(\frac{1}{N^{6-2\tau}}\right)\right]$$

$$\zeta_N(s) = \sum_{a=N+1}^{\infty} a^{-s}. \tag{48}$$

In realistic situations, when t_a are available only as numerical estimates, we evaluate such sums by splitting them into a head $\sum_{a=1}^{N} t_a$, to be evaluated directly, and the tail $R_N = \sum_{a=N+1}^{\infty} t_a$, to be estimated asymptotically in a. Now it is perhaps easier to understand the effects of pruning of the x_0 fixed point that had lead to (27). Where $\Lambda_0 \neq 1$, the fixed point approximation (47) would have been simply

$$\zeta^{(1)} = 1 - zt_1 - zt_0. \tag{49}$$

However, as $\Lambda_0 = 1$ is marginal, the effect of the x_0 fixed point is nonlinear and is probed instead by the infinity of cycles which accumulate to x_0:

$$t_0 \to t_{10} + t_{100} + t_{1000} + \ldots. \tag{50}$$

The large a behaviour of t_a can be estimated from the leading nonlinear term of the mapping at the marginal fixed point (or cycle), by the same methods as those employed in studying intermittency [31], and then the head and the tail in (47) can be matched up. In practice we find it most expedient to estimate the tail contribution by the logarithmic convergence acceleration algorithms [23,32]. How well does that work? For example, with the Levin estimate [32] for R_N, the Hausdorff dimension (I.84)

$$0 = 1 - \sum_{a=1}^{N} |\Lambda_a|^{-D_{\mathrm{H}}^{(1)}} + R_N \tag{51}$$

estimated from the first $N = 10$ fixed points is within 4% of the correct $D_{\mathrm{H}} = 1$ value

$$D_{\mathrm{H}}^{(1)} = 0.963\,396\ldots \tag{52}$$

The fixed-point estimate converges equally well for the non-trivial critical circle map irrational winding set [33]. Even though $D_{\mathrm{H}}^{(1)}$ is 4% off the correct answer, high accuracy in the determination of the fixed-points estimate $D_{\mathrm{H}}^{(1)}$ is a prerequisite for embarking upon evaluation of the curvature corrections. In contrast, without the tail estimate, the $N = 10$ truncation yields $D_{\mathrm{H}}^{(1)} = 0.89\ldots$, i.e. simple truncation of sums like (47) leads to catastrophically slow convergence (familiar from the theory of the Riemann ζ functions) of order $1/N$. The lesson is that the prerequisite to reliable computations in generic dynamical systems (systems with a mixture of hyperbolic and stable regions) are effective methods for summations over infinite families of periodic points accumulating towards marginal cycles.

6.6. Curvature corrections

In order to understand why the accuracy of the fixed-point estimate was so good, we next estimate the leading curvature correction $\hat{t}_{12} - t_1\hat{t}_2$ in (27)

$$t_{1a} - t_1 t_a = z^2 \Lambda_{1a}^{\tau}(1 - e^{\tau N_{1a}})$$

$$N_{1a} = \log \frac{\Lambda_1 \Lambda_a}{\Lambda_{1a}} = \log \Lambda_1 + 2 \log \frac{a + \sqrt{a^2+4}}{a+2+\sqrt{a(a+4)}}$$

$$= \log \Lambda_1 - \frac{4}{a} + \frac{8}{a^2} + O\left(\frac{1}{a^3}\right). \tag{53}$$

Unlike for the hyperbolic case (I.64), the nonlinearities do not fall off with cycle length, but go to a constant. This implies that every $\hat{t}_p$ counterterm series (28) has to be estimated and summed up in the same way as (47) before being included into the cycle expansion (27). Nevertheless, the curvature expansions still converge exponentially fast, for the following reason; each counterterm sequence is dominated by its head (low a terms in the $t_{\ldots a}$ series), and the head is essentially hyperbolic, as all its cycle points are far away from the marginal fixed point. For example, the leading curvature corrections to the Hausdorff dimension cycle expansion (27) are (taking $\tau = -1$):

$$\sum_{a=2}^{\infty} (\Lambda_{1a}^{\tau} - |\Lambda_1 \Lambda_a|^{\tau}) \approx 0.006\,26 + 0.008\,54 + 0.008\,15 + 0.007\,11 + 0.006\,07 + \ldots$$

to be compared with the largest term in the sum, $\Lambda_{12}^{-1} = 0.071\,79\ldots$. The first term is of order $t_{12}/\Lambda_{12} \approx 0.005\ldots$, in agreement with the hyperbolic estimate (I.64): for the successive terms the curvature cancellations increasingly fail, but the series still converges monotonically due to a crossover from a hyperbolic to a power fall-off of $\Lambda_{\ldots a} \propto a^{-2}$. The exact location of the crossover depends on the curvature series and the value of τ; for τ negative and large, the convergence is fast. As $\tau \to -1/2$, the convergence worsens; all counterterms series diverge (Riemann ζ function in (48) has a pole at $\tau = -1/2$), and the thermodynamic averages go through a phase transition [28, 34, 35] (illustrated in figure 15).

The Levin estimates from (27) truncated to $0 = 1 - \hat{t}_1 - (\hat{t}_{12} - t_1\hat{t}_2)$ and $0 = 1 - \hat{t}_1 - (\hat{t}_{12} - t_1\hat{t}_2) - (\hat{t}_{112} - t_1\hat{t}_{12})$ are respectively

$$D_H^{(2)} = 1.004\,912\ldots \qquad D_H^{(3)} = 0.997\,624\ldots.$$

and the convergence of $D_H^{(k)}$ with k is fast and in qualitative agreement with our expectations of geometric convergence. The estimates are numerically stable to 5 or 6 decimal places, but it should be noted that the numerical stability of logarithmic convergence acceleration algorithms can be rather deceptive, and better methods for evaluation of above sums are needed.

To summarise; dynamical systems with marginally stable cycles require summations of infinities of cycles accumulating to the marginal ones. If such summations are correctly carried out, the cycle expansions again converge exponentially, as long as the averaging is performed in the hyperbolic phase, i.e. the average is dominated by a positive entropy of unstable cycles. A non-trivial application of above methods to the critical circle maps mode-locking set is given in [33].

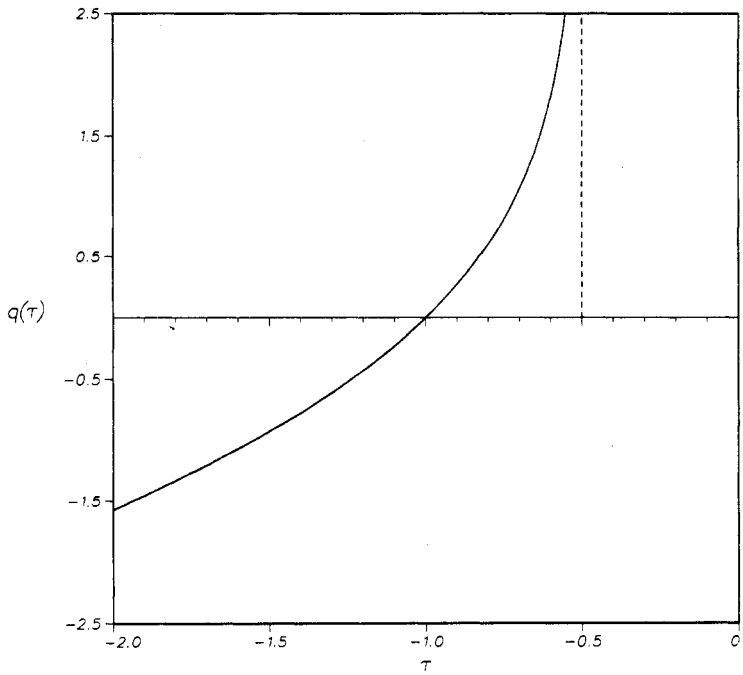

Figure 15. The function $q(\tau)$ for the 'continued fraction' thermodynamics. $D_H = 1$. For this choice of measure there is a phase transition at $\tau = -\frac{1}{2}$.

7. Summary and conclusions

We have tested here the applicability of cycle expansions on a series of low-dimensional chaotic dynamical systems. We find that the first prerequisite for convergence of cycle expansions is control of the topology (symbolic dynamics) of a dynamical system; for averages evaluated in the 'hyperbolic' phase, the effects of non-hyperbolicity play a secondary role. In other words, omitting parts of a Cantor set does more violence to averaging than approximating a smooth flow on the Cantor set by a piecewise-linear patches. Knowledge of the analytic structure of dynamical ζ functions can lead to considerable further improvement of convergence. Provided that the above requirements are met, description of sets in terms of unstable cycles can be very effective, with a few cycles yielding accurate estimates of averages over the strange set.

References

[1] Artuso R, Aurell E and Cvitanović P 1990 *Nonlinearity* **3**
[2] Ruelle D 1978 *Statistical Mechanics, Thermodynamic Formalism* (Reading, MA: Addison-Wesley)
[3] Feigenbaum M J 1988 *J. Stat. Phys.* **52** 527
[4] Lozi R 1978 *J. Physique Colloq.* **39** 9
[5] Hènon M 1976 *Commun. Math. Phys.* **50** 69
[6] Collet P and Eckmann J-P 1980 *Iterated Maps on the Interval as Dynamical Systems* (Boston: Birkhauser)
[7] Cvitanović P 1987 *Non-linear Evolution and Chaotic Phenomena* ed P Zweifel, G Gallavotti and M Anile (New York: Plenum)
[8] Sullivan D 1989 *Universality in Chaos* 2nd edn, ed P Cvitanović (Bristol: Hilger)

[9] Feigenbaum M J 1979 *J. Stat. Phys.* **21** 669
[10] Feigenbaum M J unpublished
[11] Grassberger P 1981 *J. Stat. Phys.* **26** 173
[12] Bensimon D, Jensen M H and Kadanoff L P 1986 *Phys. Rev.* A **33** 3622
[13] Aurell E 1986 *Phys. Rev.* A **34** 5135; 1987 *Phys. Rev.* A **35** 4016
[14] Kovács Z 1989 *J. Phys. A: Math. Gen.* **22** 5161
[15] Misiurewicz M 1972 *Ann. Acad. Sci., NY* **357** 348
[16] Cvitanović P, Gunaratne G H and Procaccia I 1988 *Phys. Rev.* A **38** 1503
[17] Gunaratne G H 1986 *Doctoral Thesis* Cornell University
[18] Grassberger P unpublished
[19] Grassberger P and Kantz H 1985 *Phys. Lett.* **113A** 235
[20] Ott E, Grebogi C and Yorke J A 1989 *Phys. Lett.* **135A** 343
[21] Baladi V, Eckmann J-P and Ruelle D 1989 *Nonlinearity* **2** 119
[22] Arnold R 1983 *Geometrical Methods in the Theory of Ordinary Differential Equations* (New York: Springer)
[23] Artuso R, Cvitanović P and Kenny B G 1989 *Phys. Rev.* A **39** 268
[24] Williams G T and Browne D H 1947 *Am. Math. Monthly* **54** 534
[25] MacKay R S 1982 *Doctoral Thesis* Princeton University
[26] Cvitanović P and Myrheim J 1989 *Commun. Math. Phys.* **121** 225
[27] Cvitanović P, Shraiman B and Söderberg B 1985 *Phys. Scr.* **32** 263
[28] Artuso R 1988 *J. Phys. A: Math. Gen.* **21** L923
[29] See for example Billingsley P 1965 *Ergodic Theory and Information* (New York: Wiley)
[30] Mayer D H 1976 *Bull. Soc. Math. France* **104** 195
[31] Pomeau Y and Manneville P 1980 *Commun. Math. Phys.* **74** 189
[32] Levin D 1973 *Int. J. Comput. Math.* B **3** 371
[33] Cvitanović P, Gunaratne G H and Vinson M J 1990 *Nonlinearity* **3** in press
[34] Feigenbaum M J, Procaccia I and Tél T 1989 *Phys. Rev.* A **39** 5359
[35] Csordás A and Szépfalusy P 1989 *Phys. Rev.* A **40** 2221
[36] Grassberger P 1983 *Phys. Lett.* **97A** 224
Gunaratne G H unpublished